Newton

Article

The role of magnetic dipolar interactions in skyrmion lattices

Graphical abstract

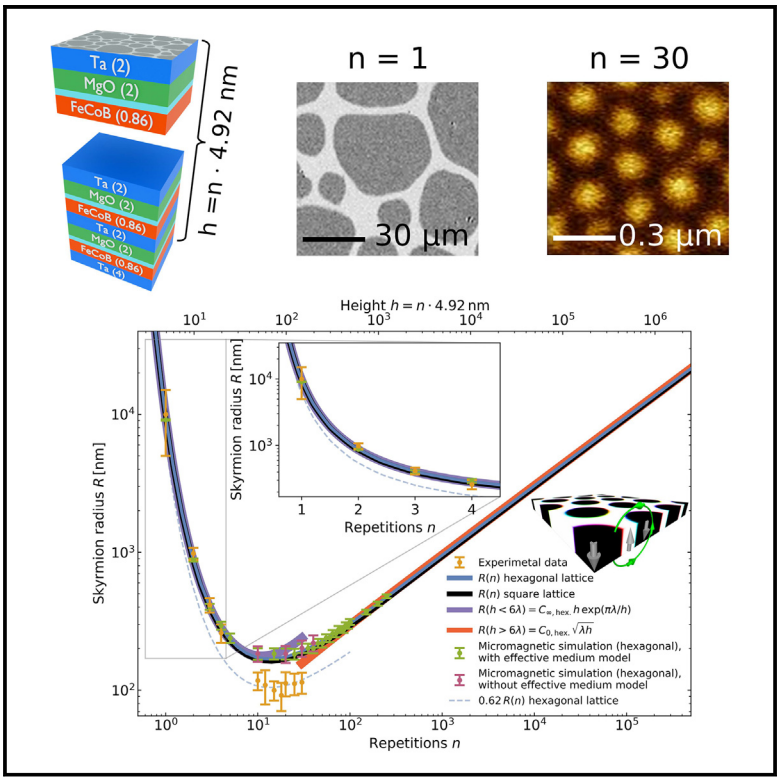

Highlights

- Skyrmion size in magnetic multilayer stacks depends on the dipolar interaction
- Dipolar interaction is tuned by varying the number of repetitions in the stack
- Analytical model describes how the size varies as a function of dipolar coupling

Authors

Elizabeth M. Jefremovas, Kilian Leutner, Miriam G. Fischer, ..., Jairo Sinova, Robert Frömter, Mathias Kläui

Correspondence

martinel@uni-mainz.de (E.M.J.), froemter@uni-mainz.de (R.F.)

In brief

Magnetic multilayer stacks can host skyrmions at room temperature and low magnetic fields, including in the form of densely packed lattices. Jefremovas et al. develop an understanding of the role of dipolar interactions in skyrmion lattices in magnetic multilayer stacks by tuning the stack repetition number, which modulates the dipolar interaction. Contrary to the case of isolated skyrmions, a stronger dipolar interaction leads to a reduction in skyrmion radius.

Jefremovas et al., 2025, Newton *1*, 100036
April 7, 2025 © 2025 The Author(s). Published by Elsevier Inc.
https://doi.org/10.1016/j.newton.2025.100036

CellPress

Newton

CellPress
OPEN ACCESS

Article

The role of magnetic dipolar interactions in skyrmion lattices

Elizabeth M. Jefremovas,[1,5,*] Kilian Leutner,[1] Miriam G. Fischer,[1] Jorge Marqués-Marchán,[2] Thomas B. Winkler,[1] Agustina Asenjo,[2] Jairo Sinova,[1,3] Robert Frömter,[1,*] and Mathias Kläui[1,4]

[1]Institute of Physics, Johannes Gutenberg University Mainz, Staudingerweg 7, 55128 Mainz, Germany
[2]Institute of Material Science of Madrid – CSIC, 28049 Madrid, Spain
[3]Department of Physics, Texas AM University, College Station, TX 77843-4242, USA
[4]Center for Quantum Spintronics, Norwegian University of Science and Technology, 7491 Trondheim, Norway
[5]Lead contact
*Correspondence: martinel@uni-mainz.de (E.M.J.), froemter@uni-mainz.de (R.F.)
https://doi.org/10.1016/j.newton.2025.100036

ACCESSIBLE OVERVIEW Magnetic skyrmions are whirling spin textures that have topological properties and are being explored for applications in memory and logic devices. They can be generated in magnetic systems, such as multilayer stacks, either as isolated units or in a lattice arrangement. In the latter case, their mutual dipolar interaction renders them an ideal platform to model and study two-dimensional (2D) inter-particle interactions. This work reveals the role of dipolar interactions in skyrmion lattices, which are strengthened upon increasing the number of repetitions of the stack, by tracking the skyrmion size and lattice periodicity as a function of the number of repetitions. Starting from magneto-optical and magnetic force microscopy imaging results, an analytical model is developed to fully capture the size dependence as a function of the number of repetitions. For the case of low repetitions, the results reveal an opposite scaling of the skyrmion size compared to the case of isolated skyrmions. The extreme sensitivity of the skyrmion size to the dipolar coupling strength in some regimes could potentially be used as a sensor in magnetic devices.

SUMMARY

Magnetic skyrmions are topological two-dimensional (2D) spin textures that can be stabilized at room temperature and low magnetic fields in magnetic multilayer stacks. Besides their envisioned applications in data storage and processing, these 2D quasiparticles constitute an ideal model system to study 2D particle properties. More precisely, the role of inter-particle dipolar interactions in 2D ensembles can be fully captured in skyrmion lattices. We engineer a multilayer stack hosting skyrmion lattices and increase the relevance of the dipolar coupling by increasing the number of repetitions n from $n = 1$ to $n = 30$. To ascertain the impact on the spin structure, we carry out a series of imaging experiments and find a drastic change of the skyrmion size. We develop an analytical description for the skyrmion radius in the whole multilayer regime, from thin to thick film limits, identifying the key impact of the nucleation process leading to the skyrmion lattice. Our work provides a detailed understanding of the skyrmion-skyrmion interaction, clarifying the role of dipolar interactions as the multilayer stack is expanded in the z direction.

INTRODUCTION

Magnetic skyrmions are non-trivial topological spin textures with promising applications in energy-efficient information storage and processing technologies.[1–8] First realized in bulk systems, such as chiral magnets,[9,10] over the last years, magnetic multilayer stacks have gained increasing attention, as they allow for tuning magnetic interactions by selecting the material parameters. In this sense, the relevant properties for spin textures, such as perpendicular magnetic anisotropy (PMA), Dzyaloshinskii-Moriya interactions (DMIs), interlayer exchange coupling, or dipolar interactions, can be tuned by selecting the materials forming the multilayer stack.[11–16]

Over the last years, different stack compositions have been reported to host room-temperature (RT) stable skyrmions, which can be nucleated at low magnetic fields and provide low pinning.[17–19] This constitutes already a step forward for the envisaged applications of skyrmions in information technologies while enabling the study of the fundamental physics governing the formation of topologically non-trivial spin structure

This is an open access article under the CC BY-NC license (http://creativecommons.org/licenses/by-nc/4.0/).

arrangements using laboratory techniques, such as Kerr microscopy or magnetic force microscopy (MFM).[6,20] Furthermore, densely packed skyrmions can also form two-dimensional (2D) lattices,[19,21] constituting an excellent playground to study 2D properties, such as dipolar inter-particle interactions, similar to 2D melting in colloidal systems.[22–24] The above-mentioned tunability of the magnetic properties by engineering the magnetic multilayer stack parameters is indeed a key advantage of skyrmions compared to their colloid counterparts.

Dipolar-stabilized skyrmions rely on the competition between long-range dipolar interactions, ferromagnetic (FM) exchange, and magnetic anisotropy.[25–29] In addition to not requiring significant DMI values, in these skyrmions, the lateral spin structure size can be significantly larger than the domain wall (DW) width Δ,[30] which often results in significantly larger topological textures (μm vs. nm) compared to DMI-stabilized ones.[31–35] This has the practical advantage that optical experimental techniques can be used for probing the textures, either statically or dynamically, under oscillating magnetic fields and/or currents,[6,21,36–38] facilitating experimental studies. In addition to this, magnetic dipolar interactions can easily be tuned in these multilayer stacks by increasing the number of repetitions of the magnetic multilayer unit, providing a wider range of coupling strengths compared to the experimentally accessible DMI values that are, as an interfacial effect, restricted by the choice of materials. Moreover, the dipolar effects make skyrmion-skyrmion interactions stronger, rendering the system an ideal candidate to probe and quantify the role of dipolar interaction in 2D lattices. Up to now, the available models in the literature have focused only on understanding the role of dipolar interactions in isolated skyrmions, where a single skyrmion can freely expand to minimize the total energy in an infinite system without being affected by the surrounding neighbors,[39] and are thus not applicable to lattices. The few recent works addressing dipolar-stabilized skyrmion lattices only provide a qualitative understanding (e.g., Zázvorka et al.,[37] Rohart and Thiaville,[40] Li et al.,[41] Vidal-Silva et al.,[42] and Leonov et al.[43]). It is remarkable how, despite the significant interest in the generation and manipulation of skyrmions in magnetic multilayer systems, fundamental aspects of the skyrmion lattice phase, disregarding the presence or absence of local or long-range order[37] like the dependence of the radius R and periodicity P on the dipolar coupling strength, have not yet been addressed.

In this work, we engineer a magnetic multilayer stack hosting skyrmion lattices at RT and zero field and vary the number of repetitions to increase the magneto-dipolar coupling. We develop an analytical model capable of accounting for the reduction of the skyrmion size as the dipolar interactions get stronger. It is worth mentioning that our stack is designed to have low pinning, which is paramount to allow the system to relax into its ground state with a very shallow energy minimum. The pinning in our films is low enough that single-repetition stacks of the same material's sequence show thermally activated skyrmion diffusion at RT, e.g., Zázvorka et al.[18] and Gruber et al.[19,21] The essential difference between our findings and preceding works on isolated skyrmion lattices is that we consider the minimum of the energy for a system where the number (or density) of skyrmions is a free parameter itself, and the skyrmion lattice is lower in energy than the FM state. For the experiment, this implies that the nucleation barrier is low and can be overcome using appropriate field protocols. We will show in the following that dipolar-stabilized skyrmions show the opposite size dependence upon increasing the number of repetitions when they arrange into lattices compared to what has been reported for an isolated skyrmion, and we explain this based on the model that we develop.

RESULTS AND DISCUSSION

Experimental observation of skyrmion lattices in multilayer stacks

We have engineered a magnetic multilayer from a Ta/CoFeB-based stack that hosts Néel skyrmions, as verified by DMI analysis and current-induced dynamics measurements previously performed in our group (e.g., in Raab et al.,[6] Gruber et al.,[21] and Zázvorka et al.[37]), as a platform for skyrmion lattices. Starting from this configuration, we have tuned the relative strength of the dipolar interactions by increasing the number of repetitions, n, from 1 to 30. A simple sketch of the stack is shown in Figure 1G. As for multilayer stacks, the metastable skyrmion lattice state is the result of the interplay between several material parameters, namely the saturation magnetization M_s, the uniaxial magnetic anisotropy K_u, the DMI strength (D), and the exchange stiffness A (Lemesh et al.[44]). To quantitatively determine M_s and K_u, we have used superconducting quantum interference device (SQUID) magnetometry. Within the experimental uncertainty, we find constant values of $M_s = 600 \pm 30$ kA/m and $K_u = 300 \pm 40$ kJ/m^3 over the whole series (see Note S1). From the observation of a constant uniaxial anisotropy, we conclude it is not significantly affected by the number of repetitions, which leads us to assume that K_u is also homogeneous over the FM layers of all individual repetition units. With the anisotropy being generally the most susceptible quantity to any structural changes at the interfaces, the constant K_u serves as a good indication to also expect a homogeneous interfacial DMI over the whole stack, i.e., independent of n. The same holds for the exchange stiffness in the unaltered local atomic environment of the CoFeB layers. Hence, we can assume a value of $A = 10$ pJ/m for this parameter, which leads to a value of $D = 0.9$ mJ/m^2 to obtain perfect quantitative agreement with our model. Both values conform well with those reported in the literature for similar stack compositions.[18,20,45] The contributions to the total energy that originate from A, D, and K_u define the DW energy and scale linearly with n, so the skyrmion size resulting from a minimization of these energy terms alone would not change with n. In contrast, the dipolar energy, depending on M_s, includes contributions from the mutual interactions between all layers and shows a more complex, non-monotonic dependence on the number of repetitions. Whereas for very thick films with a total stack thickness h significantly larger than the skyrmion radius, $h \gg R$, the explicit thickness dependence vanishes entirely, in the thin film regime ($h \ll R$), which is the regime where dipolar skyrmions are usually observed, the dipolar energy scales almost quadratically with n, as proposed by C. Kittel for stripe domains.[46] This means that, by changing n, we can selectively tune the strength of the dipolar interactions, which translates into changes of the skyrmion size.

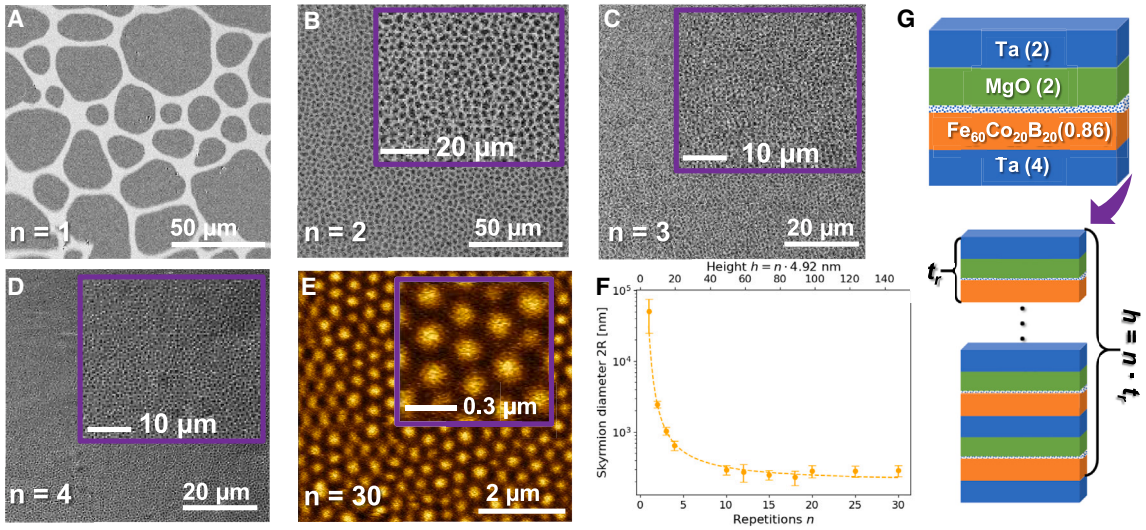

Figure 1. Skyrmion lattices in multilayer stacks

(A–D) Kerr microscopy images corresponding to $n = 1$–4 repetitions of the multilayer stack taken at room temperature (RT) and in zero external field. Light gray represents magnetization pointing in the $+z$ direction. A strong decrease of skyrmion size with increasing n is observed. Insets give higher-magnification views on the skyrmion lattices.

(E) Magnetic force microscopy (MFM) image of the $n = 30$ repetition sample taken at RT and zero external magnetic field with an ultra-low moment customized tip. Brown contrast corresponds to $+z$ magnetization. The inset shows a higher-magnification view on the hexagonal clusters.

(F) Skyrmion diameter $2R$ vs. number of repetitions, n, as extracted from the images, together with a fit to a phenomenological exponential decay, yielding $2R = ae^{b/n}$, where $a = (190 \pm 15)$ nm and $b = 5.1 \pm 0.3$. Error bars correspond to statistical standard errors from the measurements.

(G) Schematic view on the stack, with numbers in brackets indicating film thicknesses in nm. Each unit of thickness t_r is repeated n times, yielding the total height h of the stack as $h = n \cdot t_r$.

Figures 1A–1D show Kerr microscopy images of $n = 1$–4 repetitions measured at zero field, while Figure 1E includes a representative MFM image of the $n = 30$ stack. With the exception of $n = 1$, where a larger spread of sizes and shapes is observed, all the images show arrays of close-to-circular skyrmions with almost homogeneous sizes. The $n = 1$ repetition hosts $\approx$40 μm diameter skyrmions, with a significant size variation of about 50%, while the skyrmions at $n = 2$ are already a factor of 20 smaller ($\approx$2.3 μm) with a size variation below 10%. At $n = 4$, the average skyrmion diameter is 520 nm, which is close to the resolution limit of the Kerr microscope. This is why the higher repetitions (from $n = 10$ to 30) have been probed with MFM, which is capable of sensing the magnetic spin structure at nanoscale resolution. Figure 1E includes a representative image of the largest number of repetitions produced experimentally, $n = 30$, where even some hexagonally ordered clusters of skyrmions (see inset) are formed. The most striking observation is related to the conspicuous decrease of the skyrmion size as the number of repetitions increases. This decrease of the skyrmion size with increasing dipolar coupling fits to a phenomenologically motivated exponential decay, as included in Figure 1F, which agrees qualitatively with the models derived for checkerboard, stripe, and stripe domain patterns.[47–51]

This systematic decrease of the skyrmion size upon increasing the number of repetitions is exactly opposite behavior to the case of isolated skyrmions.[39] To explain such a difference, we hypothesize that the existence of neighboring skyrmions results in an effective skyrmion-skyrmion interaction mediated by dipolar interactions, which is actually an interaction term not accounted for in the isolated skyrmion model previously put forward. This skyrmion-skyrmion interaction would result effectively in an additional dipolar field for the single skyrmion under consideration, acting as an additional magnetic field aligned opposite to the magnetization of the skyrmion. As a result, the skyrmion size shrinks in the same way as it would when a Zeeman term for an external field is considered. The contribution stemming from the dipolar energy term increases more strongly than linear when the number of repetitions is increased and can be effectively reduced by increasing the density of skyrmions despite the energy cost of their DWs. To test the influence of neighboring skyrmions on final skyrmion size, we have used the model proposed by Büttner et al.,[39] including ad hoc an external magnetic field. Our experimental results are reproduced by a Zeeman field in the range of μT, in line with our hypothesis of a field generated by the neighboring skyrmions, motivating our development of a full analytical model that includes this field contribution from the other skyrmions to account for the skyrmion-skyrmion interaction. In the next section, we put forward an analytical model where the energy of the system, different for each repetition n, is minimized while taking into account both the skyrmion size and lattice periodicity. We will expand our model to the limit of $n \to \infty$ under the assumption of a vertically homogeneous magnetization. Our calculations yield excellent agreement with the experiments, as well as with the results from the micromagnetic simulation, enabling us to fully capture the physics underlying these dipolar-stabilized skyrmion lattices. We also refer the

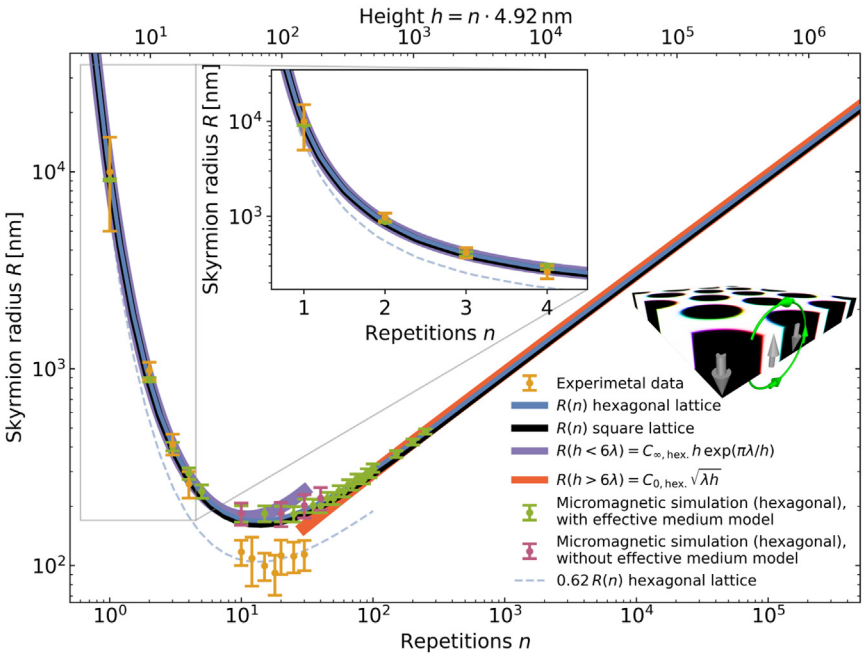

Figure 2. Skyrmion radius *R* vs. number of repetitions, *n*, in skyrmion lattices

Data points corresponding to the experiment (yellow) and micromagnetic simulation with and without the effective-medium model (green and pink, respectively). The continuous graphs represent the numerical minimization of the analytical model for arbitrary n for both hexagonal (blue) and square (black) lattices, together with the thin and thick film limits as obtained from Equation 3 (purple and orange, respectively) only for the hexagonal lattice case. Error bars indicate the experimental statistical standard errors and the estimate of the simulation accuracy resulting from the finite domain wall width and discretization. The inset zooms into the $n = 1 - 4$ range, where the agreement between simulation, model, and experimental values is excellent. Note the discrepancy with the experimental values between $n = 10$ and 30 (factor 2 smaller than the prediction), which can be reproduced by including a fitted prefactor of 0.62 (see dashed line). The sketch on the right reproduces a section from a micromagnetic simulation with the magnetization indicated by gray arrows. In addition, a field line from the front-most skyrmion to its right-hand neighbor is shown in green to illustrate how the stray field from each skyrmion acts as a reverse field on all others.

reader to the supplemental information, especially Note 3.6, where the magnetostatic energy term is fully derived for the present case of skyrmion lattice arrangements.

Analytical model for dipolar-stabilized skyrmion lattices

In order to capture the physics underneath skyrmion lattices, we have developed an analytical model capable of providing a description of the skyrmion size and periodicity. Our model assumes skyrmions arranged in a lattice with periodicity P as rigid circular cylinders with radius R and height h centered at the skyrmion center, which extend across all layers. We consider skyrmions with radius R and DW width Δ under the condition $R \gg \Delta$. The magnetization configuration of the wall follows a Néel-type profile.[52–54] To reduce the computational costs, we treat the full stack as a single homogeneous magnetic layer using the effective medium model introduced in Woo et al.[55] (green dots in Figure 2). The validity of this approach is discussed in the supplemental information (see Note 2) and can be easily checked by following the pink dots in Figure 2, which show the results of the full micromagnetic calculations treating all layers individually.

In the following, we will introduce the expressions for the energy terms in a skyrmion lattice assuming both square and hexagonal skyrmion arrangements, for which we consider the total energy density ϵ per unit cell as the sum of the contributions from DW and magnetostatic energies:

$$\epsilon(\Delta, R, P) = \frac{1}{A_{\mathrm{uc}}}\left[2\pi R h \sigma_{\mathrm{DW}}(\Delta) + E_{\mathrm{f}}(P) + E_{\mathrm{c}}(R) + E_{\mathrm{c}\leftrightarrow\mathrm{f}}(R) + E_{\mathrm{c}\leftrightarrow\mathrm{c}}(R, P)\right] \quad \text{(Equation 1)}$$

In this expression, σ_{DW} represents the DW energy density of the skyrmion per unit wall area. The terms arising from the magnetostatic energy are the following: $E_{\mathrm{f}}(P)$ is the self-energy contribution of the homogeneously magnetized film within the considered unit cell, $E_{\mathrm{c}}(R)$ is the self-energy of an isolated homogeneously magnetized cylinder, $E_{\mathrm{c}\leftrightarrow\mathrm{f}}(R)$ represents the interaction between the cylinder and the FM film, and $E_{\mathrm{c}\leftrightarrow\mathrm{c}}(R, P)$ describes the interaction between the cylinder in the considered unit cell and all other cylinders in the lattice. Note that these energy terms are divided by $A_{\mathrm{uc}} \sim P^2$, the area of the unit cell, to obtain ϵ. The main innovation of our model concerns the analytical treatment of the interaction between the cylinder in the considered unit cell with all other cylinders, $E_{c\leftrightarrow c}$. To perform this calculation, we proceed in two steps: first, the interaction energy between two individual cylinders, $E_{s,c\leftrightarrow c}$, is calculated via a multipole expansion. Second, $E_{s,c\leftrightarrow c}$ is summed over all the cylinders in the lattice, excluding the cylinder in the considered unit cell. This sum is a 2D infinite series, which is estimated to be a good approximation using the Euler-Maclaurin formula,[56] which has also been recently applied to calculate two-skyrmion system energies.[57] In this way, the influence of the complete lattice is captured. The detailed derivation is explained in the supplemental information, along with the remaining terms arising from the magnetostatic energy.

To calculate the DW energy density, σ_{DW}, we first decompose it into the following independent contributions:

$$\sigma_{\mathrm{DW}}(\Delta, h) = \frac{E_{\mathrm{ex}} + E_{\mathrm{a}} + E_{\mathrm{DMI}} + E_{\rho\rho} + E_{\sigma\sigma,\mathrm{nc}}}{2\pi R h} \quad \text{(Equation 2)}$$

This includes exchange E_{ex}, anisotropy E_a, and DMI E_{DMI} energy terms, along with $E_{\rho\rho}$, which is the energy of the volume charges arising in the whole volume of the DW, and $E_{\sigma\sigma,nc}$, which is the energy due to the deviation of surface charges from the cylinder lattice caused by the finite DW width Δ. A more detailed explanation on these terms is provided in the supplemental information. Note that Δ depends on neither R nor P, as $\Delta \ll R$, so the curvature of the DW can, in practice, be neglected for the relatively large dipolar skyrmions. This implies that $\sigma_{DW}(\Delta, h)$ can actually be numerically minimized to obtain the equilibrium value $\Delta_0(h)$ as a function of h before considering the minimization of the other terms in ϵ. Actually, the variation of $\Delta_0(h)$ with h is quite weak. Taking the material parameters of our system, Δ_0 varies from $\Delta_0(h \to 0) = 11.6$ nm to $\Delta_0(h \to \infty) = 8.1$ nm. These values agree with the ones reported for similar systems.[39,52]

Finally, to calculate the equilibrium values for the radius R_0 and the periodicity P_0, the energy density ϵ is minimized, which implies solving $(R_0, P_0) = \min_{R,P} \epsilon(\Delta_0, R, P)$. To enable further analytical treatment, a simplification can be made provided the absence of external fields, which conforms to the condition in our experiments. For this case, we can assume that the area filling of the skyrmion and the FM background are equal, giving rise to surface-charge neutrality on both top and bottom surfaces in order to minimize ϵ. This yields the relations $P = 2R\sqrt{\pi}/\sqrt[4]{3}$ for the hexagonal lattice and $P = R\sqrt{2\pi}$ for the square lattice. With this, we derive a closed analytical solution for the equilibrium value of R_0 in the two regimes $h \ll 6\lambda$ (thin-film regime) and $h \gg 6\lambda$ (thick-film regime) for the hexagonal and square skyrmion lattices, $\lambda = \sigma_{DW}/\mu_0 M_s^2$:

$$R_0(h) = \begin{cases} C_\infty\, h \exp\left(\dfrac{\pi\lambda}{h}\right) & h \ll 6\lambda \\ C_0\sqrt{\lambda h} & h \gg 6\lambda \end{cases} \qquad \text{(Equation 3)}$$

with $C_{\infty,hex.} = 0.976$ and $C_{0,hex.} = 2.646$ for the hexagonal lattice and $C_{\infty,sq.} = 1.019$ and $C_{0,sq.} = 2.580$ for the square lattice. The characteristic length is calculated from $\sigma_{DW} = \sigma_{DW}(\Delta_0(h))$ using the previously determined $\Delta_0(h)$. In our systems, the threshold between the regimes $h = 6\lambda$ corresponds to $n = 30$.

In the regime $h \ll 6\lambda$, Equation 3 has the same scaling behavior as previously derived for the stripe and checkerboard domains in Kaplan and Gehring,[47] Málek and Kamberský,[49] Millev,[50] and Kooy.[58] The $h \gg 6\lambda$ limit, which predicts an increase in skyrmion size with a large number of repetitions, has the same scaling as the Kittel model for periodic stripe domains.[46] Indeed, the prefactors we find for skyrmion lattices are different from the ones derived for stripe domains. To validate the assumption of charge neutrality that we made for the field-free case, we numerically minimized $(R_0, P_0) = \min_{R,P} \epsilon(\Delta_0, R, P)$ without assuming magnetic charge neutrality to obtain $R_0(h)$ for arbitrary h. The ratio R_0/P_0 deviates by, at maximum, 3% from the ratio obtained under the charge neutrality assumption for arbitrary h from the thin-film to the thick-film region.

Figure 2 includes the predictions from our model, the analytical formulas for the hexagonal lattice in both limits from Equation 3, and the results from the numerical minimization of $\epsilon(\Delta, R, P)$ for both square and hexagonal lattices, as well as the experimental results shown in Figure 1F. A plot with the analytical formulas for both limits of the square lattice in Equation 3 is provided in the supplemental information. We have also added values for the skyrmion sizes derived from micromagnetic simulations (details on the simulations are included in the supplemental information, Note S4). The simulations have been carried out both in the effective-medium model (green dots in Figure 2) and using the full stack of individual, decoupled layers (dark pink dots in Figure 2). Both simulation sets coincide, validating the use of the effective-medium model for our system.

As observed in Figure 2, the model reproduces very well the decrease of the skyrmion size as a function of the number of repetitions for $n \leq 4$, matching both the experimental and simulation results. Toward the thick-film regime $h \gg 6\lambda$, the model predicts an increase of the skyrmion size, which is beyond the range accessible in our experiments but is also reproduced by our numerical simulations. There is, however, a clear discrepancy between the experimental values and the model and simulations in the regime around the skyrmion minimum size, from $n = 10$ to 30, where the observed skyrmions are about a factor 2 smaller than predicted from energy minimization. The reason for this discrepancy, which is consistent in all measurements from $n = 10$ to 30, concerns the specific nucleation mechanism of the skyrmion lattice and will be discussed in detail in the next section.

Nucleation of overfilled skyrmion lattices from the stripe phase

As observed in Figure 2, in the regime around the skyrmion minimum size, i.e., from $n = 10$ to 30, the experimental values for the skyrmion size are a factor of ≈ 2 smaller compared to the numerical values. We have evaluated several scenarios that could lead to such a deviation. First, we considered the possibility that skyrmions may actually deviate from a perfect rigid skyrmion tube shape across the multilayer, resulting in a flower-vase-like tube, which would yield a decrease in the skyrmion size at the top and bottom surfaces. This scenario has recently been discussed by Srivastava et al. for $n = 20$ repetitions in a FeCoB-based stack.[59] However, none of our simulations (without using the effective-medium model) showed significant deviations (below 5%) of the skyrmion radius across the multilayer (see the supplemental information and Figures S7 and S8 therein). Our simulations also rule out the hybrid-skyrmion scenario, observed in Fe/Gd multilayers, for which the weak PMA results in a Néel-Bloch-Néel skyrmion tube across the stack,[60,61] or in Legrand,[62] where hybrid chiral DWs are promoted from the interlayer exchange. We can also exclude the factor 2 difference as an artifact from MFM imaging. Although the stray field of the MFM tip could, in principle, locally evoke a reduction in skyrmion size, we can exclude a significant influence of the tip magnetic field on the sample, as we do not observe sudden changes in the skyrmion lattice from one scan line to the next. This excludes already stochastic reconfigurations of the skyrmion lattice triggered by the local proximity of the tip and, hence, from the tip's stray field. Very likely, the lattice, with its long-range mutual dipolar interactions, is much more robust compared to an isolated skyrmion. Moreover, the presence of a localized external

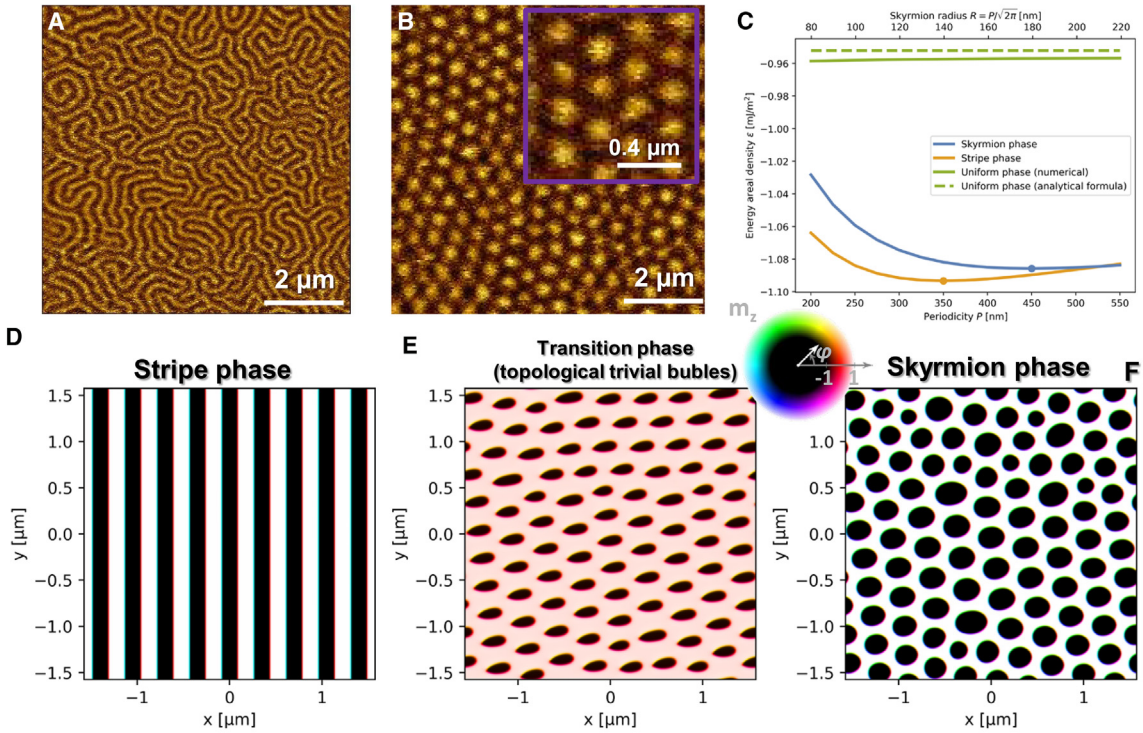

Figure 3. Stripe-to-skyrmion transition

(A and B) Representative MFM images of a multilayer with $n = 15$ after out-of-plane and in-plane saturation, respectively. Note the difference in the periodicity between the maze domain pattern in (A) and the skyrmion lattice in (B), with the presence of local hexagonal order zoomed-in in the inset.

(C) The areal energy density for the uniform, stripe, and skyrmion phases is plotted vs. the periodicity. The stripe phase is the lowest energy state for all the experimentally observed periodicities. The dots indicate the minima in the energy areal density.

(D–F) Three successive states from a micromagnetic simulation showing the nucleation process of a skyrmion lattice (F) from the stripe-domain phase (D), mediated via topologically trivial bubble domains (E). The dataset is obtained by minimizing the total energy of the system under continuous linear field variation, starting from an initial state at zero field (left) via an applied field of $\mu_0 H$ = (150 mT, 0, 20 mT) (middle) back to zero field (right). The magnetic contrast is encoded according to the color wheel.

magnetic field above the skyrmion could, in principle, give rise to a gradual and reversible continuous deformation of the skyrmion lattice directly under it. However, given that in this scenario, no nucleation or annihilation of skyrmions occurs, this would not alter the lattice periodicity over the whole scan range of an image, which is the actual parameter used to determine the skyrmion radius from the MFM measurements. Taking all this into account, we propose a dynamic effect occurring during the nucleation of the spin textures from stripes to skyrmions as the most likely explanation for the factor 2 deviation.

Figure 3A shows a representative MFM image, taken at zero field, of the $n = 15$ sample after applying a 135 mT out-of-plane (OOP) field, which is sufficient to saturate the stack (see magnetization characterization in Note S1). When the field is removed, the magnetization relaxes back to a stripe-domain state. Note the maze-like pattern, which, together with the occurrence of areas with local hexagonal order, indicates the low pinning of the samples.[63] The periodicity extracted from the MFM images (2D-fast Fourier transform [FFT]) corresponds to (300 ± 30) nm for all $n = 10$–30. If we now change the geometry of the field in such a way that we combine a strong in-plane (IP) component (135 mT) with a small OOP component (below 20 mT), we observe that the magnetization undergoes a transition to a skyrmion lattice phase, adopting the arrangement shown in Figure 3B. To better understand this transition, we have plotted in Figure 3C the calculated energy areal density corresponding to both the stripe and skyrmion phases. As can be seen, both energy minima are close in energy and well below the one corresponding to the uniform phase. Note, however, that while the calculated energy minimum for the stripe phase (350 nm in $n = 15$) is close to our experimental finding, (290 ± 20) nm, there is a factor 2 difference between the calculated energy minimum for skyrmions (450 nm) and the experimentally observed value, (250 ± 40) nm. This factor 2 difference, already observed in the analytical model presented in Figure 2 in the previous section, can be understood by diving into the nucleation process, which is possible thanks to micromagnetic simulations.

Based on micromagnetic simulations, we propose a mechanism that enables the transition from the stripe to the skyrmion lattice phase through an intermediate phase of topologically trivial bubble domains. Starting from a stripe-domain configuration with all domains perfectly aligned, as pictured in Figure 3D, we apply an IP field of 150 mT at 90° ± 15° relative to the stripe direction with a small OOP component (20 mT, which corresponds

to ≈6° OOP). Under the influence of this field, the stripes deform and finally break up, forming an intermediate phase consisting of topological trivial bubbles with zero topological charge ($Q = 0$), as shown in Figure 3E. We would like to point out that these bubbles are not akin to the skyrmion-antiskyrmion droplets recently reported.[64] In our case, the bubbles exhibit Néel and Bloch walls at the same time, unlike the skyrmion-antiskyrmion droplets. According to our simulations, these bubbles are not stable in the absence of an IP field and evolve to the final metastable skyrmion lattice (see Figure 3F) with a topological charge $Q = 1$ per skyrmion when the field is removed. This resulting skyrmion lattice does not arrive, however, at the very shallow energy minimum of the system, yet it ends in a local metastable minimum, corresponding to an *overfilled* configuration, as the annihilation barrier of the skyrmions is too high to overcome. This overfilled configuration consists of a higher density of smaller skyrmions compared to the one corresponding to the equilibrium state of the global energy minimum, which is the one calculated and shown in Figure 2. This has, in fact, a crucial impact on the lattice periodicity, as the overcrowded skyrmion lattice has a much smaller periodicity (calculated values between 250 and 300 nm for $n = 10$–30) than the equilibrium skyrmion lattice (around 500 nm). The different nucleation protocol for the case of low repetitions ($n = 1$–4), where we combined the OOP with an IP pulse, drives the experimentally obtained skyrmion lattice to the actual global energy minimum. Note that this difference of just a factor 2 is visible clearly in our experiments thanks to the careful design of the multilayer stack, as the $n = 10$–30 repetitions have sufficiently steep energy minima (large curvature of the energy landscape) to lead to the deviations from the calculated periodicity.

Conclusions

In this work, we have systematically studied the role of dipolar interactions in skyrmion lattices at equilibrium, elucidating the role of both skyrmion size and lattice periodicity in minimizing the energy density of the system. Our results reveal an opposite scaling of the skyrmion size with the number of repetitions of the FM layer compared to the case of isolated skyrmions. This finding can be attributed to a stronger-than-linear increasing contribution of the dipolar energy with the number of repetitions, which can be effectively reduced by increasing the density of skyrmions despite the energy cost of their DWs. The model that we derived to describe this low-repetition range reproduces the same scaling previously derived for stripe domains[47,48] but with a prefactor. With the parameters of our material, this behavior is found over the range of repetitions from $n = 1$ to 10, which is typically realized in experiments nowadays. The reduction of the skyrmion size with increasing n in this low-repetition regime constitutes an asset for implementing skyrmion lattices in spintronic devices, as it enables achieving larger densities of skyrmions whose stability over external fields and/or temperature variations is also increased. Following a region with almost constant skyrmion size, which, in our system, comprises from 10 to 30 repetitions, at the high-repetition range, this dependence inverts so that the skyrmion radius increases with the square root of the thickness, reproducing the scaling of the Kittel model for stripe domains.[46] In addition to these equilibrium considerations, we also describe a transient nucleation mechanism for a skyrmion lattice starting from a stripe domain state, elucidating the key role of the initial stripe periodicity on the final skyrmion lattice density (overfilled lattice vs. not overfilled).

Our designed stack shows remarkably low pinning all over the number of repetitions, which is key for achieving the ground state and understanding the critical influence of the dipolar interactions in such 2D lattice arrangements. As a future direction, it can be envisioned to study the 2D transitions (solid-hexatic-nematic) of such 2D skyrmion lattices as a function of the number of repetitions, n, to determine the influence of the skyrmion-skyrmion dipolar interactions in the melting of the lattice. Beyond the static regime, our system is also ideal for future dynamic studies, where the impact of the dipolar term in collective skyrmion motion, such as current-induced dynamics and/or the skyrmion Hall effect, in $n > 1$ multilayer stacks, is expected to also lead to interesting collective phenomena.[65]

Our work also provides a nucleation mechanism that enables the transition from stripes to skyrmions at RT and with magnetic fields in the mT regime, obtaining overfilled skyrmion lattices, by the rotation of the IP field. This opens up a very simple experimental procedure to increase the lattice density. Finally, it is worth mentioning there is an extremely sensitive size decrease of the skyrmions at low dipolar coupling, which could be used as an indicator to monitor the dipolar coupling in magnetic tunnel junctions (MTJs) or current-induced motion of skyrmions in devices (e.g., race-track memories, as introduced in Fert et al.[2]). In this way, inhomogeneities in the dipolar field, caused by the interactions with the different components, would be detectable by imaging the skyrmion size and shape.

METHODS

Experimental procedures

Magnetic multilayer stacks of the form Ta(4)/[$Co_{20}Fe_{60}B_{20}$(0.86)/Ta(0.06)/MgO(2)/Ta(2)] ×n (layer thicknesses in nm, 0.01 nm precision), with n being the number of repetitions, were deposited using a Singulus Rotaris magnetron sputtering tool with a base pressure of 3×10^{-8} mbar onto Si/SiO_2 substrates. The surface roughness of the films (root mean square [rms]) was determined by atomic force microscopy (AFM) to be below 1 nm. To reduce the strong PMA induced at the interface between $Co_{20}Fe_{60}B_{20}$ and MgO and thus enable skyrmion nucleation at RT, a dusting layer of Ta is introduced between them. The randomly distributed Ta atoms weaken the Fe–O and Co–O bonds, reducing the PMA of the stack.[66] The increase in dipolar energy density has been achieved by increasing the number of repetitions, n.

Hysteresis M vs. H loops were performed using a SQUID for both IP and OOP configurations at RT and for fields between −2 and 2 T.

Magnetic contrast was established using the polar magneto-optical Kerr effect (MOKE) in a commercially available Kerr microscope from Evico Magnetics. Electromagnetic coils allow for the simultaneous application of OOP and IP fields up to 13 and 120 mT, respectively. The microscope was set up in a thermally stabilized flow box, ensuring constant 292 K temperature conditions. Data were acquired with a charge-coupled device (CCD) camera as grayscale images. Skyrmions were nucleated

in a constant OOP field, from ≈100 μT for $n = 1$ to ≈ 6 mT for $n = 4$, by applying a saturating IP field pulse of ≈0.5 s duration, in the same way as in Gruber et al.[19] and Zázvorka et al.[37] All images shown and discussed in the present work are taken at zero field (both IP and OOP). Skyrmion sizes were determined from the images by machine-learning-based detection using U-Net[67] and cross-checked by ImageJ.[68]

MFM and the corresponding AFM images were recorded using a Nanotec scanning probe microscopy system controlled by WSxM software.[69] In order to minimize the influence of the tip magnetic moment on the sample, customized ultra-low moment tips were produced. For this, a thin film of Co (≈10 nm) was deposited onto the front face of a commercial Nanosensors PPP-FMR tip. This ultra-low coating thickness[70] ensured a proficient signal-to-noise ratio during the measurements, carried out in amplitude modulation mode.

Numerical simulations

Micromagnetic simulations were performed using MuMax 3.[71] Additionally, the simulations were conducted by treating each magnetic layer individually, as well as by modeling the multilayer stack as a single-layer homogeneous ferromagnet, following the effective medium model.[55] In this approach, the parameters M_s, A, K, and D were scaled accordingly. A discretization of $\Delta x = \Delta y = 5$ nm was employed. A hexagonal skyrmion lattice was simulated, with the simulated area having lengths of $l_x = P$ in the x direction and $l_y = \sqrt{3}P$ in the y direction. Periodic boundary conditions were applied in both the x and y directions. Technical details and further information are included in the supplemental information.

RESOURCE AVAILABILITY

Lead contact

Requests for further information and resources should be directed to and will be fulfilled by the corresponding authors, Elizabeth M. Jefremovas (lead contact; martinel@uni-mainz.de) and Robert Frömter (froemter@uni-mainz.de).

Materials availability

Materials are available upon reasonable request to the corresponding authors, Elizabeth M. Jefremovas and Robert Frömter.

Data and code availability

The authors confirm that the data supporting the findings of this study are available within the article and/or its supplemental information. The codes are available upon reasonable request to the corresponding authors, Elizabeth M. Jefremovas and Robert Frömter.

ACKNOWLEDGMENTS

E.M.J. acknowledges the Alexander von Humboldt Postdoctoral Fellowship. Support from DFG (Priority Program Skyrmionics grant no. 403502522 and TRR 173-268565370 Spin+X: A01, A11, B02 grant no. 358671374), the European Research Council (ERC) under the European Union's Horizon 2020 research and innovation program (grant no. 856538, project "3D MAGiC"), and Horizon Europe project NIMFEIA (grant no. 101070290) is acknowledged. This research is part of the TOPOCOM project, which is funded by the European Union's Horizon Europe Programme Horizon 1.2 under the Marie Skłodowska-Curie Actions (MSCA), grant agreement no. 101119608. M.K. acknowledges the Research Council of Norway through its Centers of Excellence funding scheme, project no. 262633 "QuSpin."

AUTHOR CONTRIBUTIONS

E.M.J. conceived the experiments; K.L. carried out the theoretical and micromagnetic calculations; E.M.J., M.G.F., and J.M.-M. conducted and analyzed the experiments; K.L. and R.F. developed the theoretical model; and R.F. and M.K. supervised the project. All authors reviewed and contributed to the writing of the manuscript.

DECLARATION OF INTERESTS

J.S. is a member of *Newton* scientific advisory board.

SUPPLEMENTAL INFORMATION

Supplemental information can be found online at https://doi.org/10.1016/j.newton.2025.100036.

Received: October 25, 2024
Revised: January 10, 2025
Accepted: February 24, 2025
Published: March 24, 2025

REFERENCES

1. Bogdanov, A.N., and Panagopoulos, C. (2020). Physical foundations and basic properties of magnetic skyrmions. Nat. Rev. Phys. *2*, 492–498.
2. Fert, A., Reyren, N., and Cros, V. (2017). Magnetic skyrmions: advances in physics and potential applications. Nat. Rev. Mater. *2*, 17031–17115.
3. Everschor-Sitte, K., Masell, J., Reeve, R.M., and Kläui, M. (2018). Perspective: Magnetic skyrmions—overview of recent progress in an active research field. J. Appl. Phys. *124*.
4. Nagaosa, N., and Tokura, Y. (2013). Topological properties and dynamics of magnetic skyrmions. Nat. Nanotechnol. *8*, 899–911.
5. Brems, M.A., Kläui, M., and Virnau, P. (2021). Circuits and excitations to enable brownian token-based computing with skyrmions. Appl. Phys. Lett. *119*.
6. Raab, K., Brems, M.A., Beneke, G., Dohi, T., Rothörl, J., Kammerbauer, F., Mentink, J.H., and Kläui, M. (2022). Brownian reservoir computing realized using geometrically confined skyrmion dynamics. Nat. Commun. *13*, 6982.
7. Song, K.M., Jeong, J.-S., Pan, B., Zhang, X., Xia, J., Cha, S., Park, T.-E., Kim, K., Finizio, S., Raabe, J., et al. (2020). Skyrmion-based artificial synapses for neuromorphic computing. Nat. Electron. *3*, 148–155.
8. Leutner, K., Winkler, T.B., Gruber, R., Frömter, R., Güttinger, J., Fangohr, H., and Kläui, M. (2023). Skyrmion automotion and readout in confined counter-sensor device geometries. Phys. Rev. Appl. *20*, 064021.
9. Tokura, Y., and Kanazawa, N. (2021). Magnetic skyrmion materials. Chem. Rev. *121*, 2857–2897.
10. Mühlbauer, S., Binz, B., Jonietz, F., Pfleiderer, C., Rosch, A., Neubauer, A., Georgii, R., and Böni, P. (2009). Skyrmion lattice in a chiral magnet. Science *323*, 915–919.
11. Dupé, B., Bihlmayer, G., Böttcher, M., Blügel, S., and Heinze, S. (2016). Engineering skyrmions in transition-metal multilayers for spintronics. Nat. Commun. *7*, 11779.
12. Soumyanarayanan, A., Raju, M., Gonzalez Oyarce, A.L., Tan, A.K.C., Im, M.-Y., Petrović, A.P., Ho, P., Khoo, K.H., Tran, M., Gan, C.K., et al. (2017). Tunable room-temperature magnetic skyrmions in Ir/Fe/Co/Pt multilayers. Nat. Mater. *16*, 898–904.
13. Dohi, T., Reeve, R.M., and Kläui, M. (2022). Thin film skyrmionics. Annu. Rev. Condens. Matter Phys. *13*, 73–95.
14. Jiang, W., Chen, G., Liu, K., Zang, J., Te Velthuis, S.G., and Hoffmann, A. (2017). Skyrmions in magnetic multilayers. Phys. Rep. *704*, 1–49.

15. Satywali, B., Kravchuk, V.P., Pan, L., Raju, M., He, S., Ma, F., Petrović, A.P., Garst, M., and Panagopoulos, C. (2021). Microwave resonances of magnetic skyrmions in thin film multilayers. Nat. Commun. *12*, 1909.

16. Yuan, F.-T., Lin, Y.-H., Mei, J., Hsu, J.-H., and Kuo, P. (2012). Effect of thickness of Mgo, Co-Fe-B, and ta layers on perpendicular magnetic anisotropy of [Ta/$Co_{60}Fe_{20}B_{20}$/MgO]x5 multilayered films. J. Appl. Phys. *111*.

17. Zhou, Y., Mansell, R., and van Dijken, S. (2021). Voltage control of skyrmions: Creation, annihilation, and zero-magnetic field stabilization. Appl. Phys. Lett. *118*.

18. Zázvorka, J., Jakobs, F., Heinze, D., Keil, N., Kromin, S., Jaiswal, S., Litzius, K., Jakob, G., Virnau, P., Pinna, D., et al. (2019). Thermal skyrmion diffusion used in a reshuffler device. Nat. Nanotechnol. *14*, 658–661.

19. Gruber, R., Brems, M.A., Rothörl, J., Sparmann, T., Schmitt, M., Kononenko, I., Kammerbauer, F., Syskaki, M.-A., Farago, O., Virnau, P., and Kläui, M. (2023). 300-times-increased diffusive skyrmion dynamics and effective pinning reduction by periodic field excitation. Adv. Mater. *35*, 2208922.

20. Casiraghi, A., Corte-León, H., Vafaee, M., Garcia-Sanchez, F., Durin, G., Pasquale, M., Jakob, G., Kläui, M., and Kazakova, O. (2019). Individual skyrmion manipulation by local magnetic field gradients. Commun. Phys. *2*, 145.

21. Gruber, R., Zázvorka, J., Brems, M.A., Rodrigues, D.R., Dohi, T., Kerber, N., Seng, B., Vafaee, M., Everschor-Sitte, K., Virnau, P., and Kläui, M. (2022). Skyrmion pinning energetics in thin film systems. Nat. Commun. *13*, 3144.

22. Alert, R., Casademunt, J., and Tierno, P. (2014). Landscape-inversion phase transition in dipolar colloids: Tuning the structure and dynamics of 2D crystals. Phys. Rev. Lett. *113*, 198301.

23. Zahn, K., Lenke, R., and Maret, G. (1999). Two-stage melting of paramagnetic colloidal crystals in two dimensions. Phys. Rev. Lett. *82*, 2721–2724.

24. Keim, P., Maret, G., Herz, U., and von Grünberg, H.-H. (2004). Harmonic lattice behavior of two-dimensional colloidal crystals. Phys. Rev. Lett. *92*, 215504.

25. Montoya, S.A., Couture, S., Chess, J.J., Lee, J.C.T., Kent, N., Henze, D., Sinha, S.K., Im, M.-Y., Kevan, S.D., Fischer, P., et al. (2017). Tailoring magnetic energies to form dipole skyrmions and skyrmion lattices. Phys. Rev. B *95*, 024415.

26. Desautels, R.D., DeBeer-Schmitt, L., Montoya, S.A., Borchers, J.A., Je, S.-G., Tang, N., Im, M.-Y., Fitzsimmons, M.R., Fullerton, E.E., and Gilbert, D.A. (2019). Realization of ordered magnetic skyrmions in thin films at ambient conditions. Phys. Rev. Mater. *3*, 104406.

27. Hrabec, A., Sampaio, J., Belmeguenai, M., Gross, I., Weil, R., Chérif, S.M., Stashkevich, A., Jacques, V., Thiaville, A., and Rohart, S. (2017). Current-induced skyrmion generation and dynamics in symmetric bilayers. Nat. Commun. *8*, 15765.

28. Zhang, J., Zhang, X., Chen, H., Guang, Y., Zeng, X., Yu, G., Zhang, S., Liu, Y., Feng, J., Zhao, Y., et al. (2020). Formation and magnetic-field stability of magnetic dipole skyrmions and bubbles in a ferrimagnet. Appl. Phys. Lett. *116*.

29. Heigl, M., Koraltan, S., Vaňatka, M., Kraft, R., Abert, C., Vogler, C., Semisalova, A., Che, P., Ullrich, A., Schmidt, T., et al. (2021). Dipolar-stabilized first and second-order antiskyrmions in ferrimagnetic multilayers. Nat. Commun. *12*, 2611.

30. Ezawa, M. (2010). Giant skyrmions stabilized by dipole-dipole interactions in thin ferromagnetic films. Phys. Rev. Lett. *105*, 197202.

31. Yuan, H.Y., and Wang, X.R. (2016). Skyrmion creation and manipulation by nano-second current pulses. Sci. Rep. *6*, 22638.

32. Iwasaki, J., Mochizuki, M., and Nagaosa, N. (2013). Universal current-velocity relation of skyrmion motion in chiral magnets. Nat. Commun. *4*, 1463.

33. Zhou, Y., and Ezawa, M. (2014). A reversible conversion between a skyrmion and a domain-wall pair in a junction geometry. Nat. Commun. *5*, 4652.

34. Li, J., Tan, A., Moon, K.W., Doran, A., Marcus, M.A., Young, A.T., Arenholz, E., Ma, S., Yang, R.F., Hwang, C., and Qiu, Z.Q. (2014). Tailoring the topology of an artificial magnetic skyrmion. Nat. Commun. *5*, 4704.

35. Jiang, W., Upadhyaya, P., Zhang, W., Yu, G., Jungfleisch, M.B., Fradin, F.Y., Pearson, J.E., Tserkovnyak, Y., Wang, K.L., Heinonen, O., et al. (2015). Blowing magnetic skyrmion bubbles. Science *349*, 283–286.

36. Dohi, T., DuttaGupta, S., Fukami, S., and Ohno, H. (2019). Formation and current-induced motion of synthetic antiferromagnetic skyrmion bubbles. Nat. Commun. *10*, 5153.

37. Zázvorka, J., Dittrich, F., Ge, Y., Kerber, N., Raab, K., Winkler, T., Litzius, K., Veis, M., Virnau, P., and Kläui, M. (2020). Skyrmion lattice phases in thin film multilayer. Adv. Funct. Mater. *30*, 2004037.

38. Jefremovas, E.M., Kent, N., Marqués-Marchán, J., Fischer, M.G., Asenjo, A., and Kläui, M. (2024). Experimental realization of metastable target skyrmion states in continuous films. Appl. Phys. Lett. *125*.

39. Büttner, F., Lemesh, I., and Beach, G.S.D. (2018). Theory of isolated magnetic skyrmions: From fundamentals to room temperature applications. Sci. Rep. *8*, 4464.

40. Rohart, S., and Thiaville, A. (2013). Skyrmion confinement in ultrathin film nanostructures in the presence of dzyaloshinskii-moriya interaction. Phys. Rev. B *88*, 184422.

41. Li, W., Bykova, I., Zhang, S., Yu, G., Tomasello, R., Carpentieri, M., Liu, Y., Guang, Y., Gräfe, J., Weigand, M., et al. (2019). Anatomy of skyrmionic textures in magnetic multilayers. Adv. Mater. *31*, 1807683.

42. Vidal-Silva, N., Riveros, A., and Escrig, J. (2017). Stability of neel skyrmions in ultra-thin nanodots considering dzyaloshinskii-moriya and dipolar interactions. J. Magn. Magn Mater. *443*, 116–123.

43. Leonov, A.O., Monchesky, T.L., Romming, N., Kubetzka, A., Bogdanov, A.N., and Wiesendanger, R. (2016). The properties of isolated chiral skyrmions in thin magnetic films. New J. Phys. *18*, 065003.

44. Lemesh, I., Litzius, K., Böttcher, M., Bassirian, P., Kerber, N., Heinze, D., Zázvorka, J., Büttner, F., Caretta, L., Mann, M., et al. (2018). Current-induced skyrmion generation through morphological thermal transitions in chiral ferromagnetic heterostructures. Adv. Mater. *30*, 1805461.

45. Ge, Y., Rothörl, J., Brems, M.A., Kerber, N., Gruber, R., Dohi, T., Kläui, M., and Virnau, P. (2023). Constructing coarse-grained skyrmion potentials from experimental data with iterative boltzmann inversion. Commun. Phys. *6*, 30.

46. Kittel, C. (1946). Theory of the structure of ferromagnetic domains in films and small particles. Physiol. Rev. *70*, 965–971.

47. Kaplan, B., and Gehring, G. (1993). The domain structure in ultrathin magnetic films. J. Magn. Magn Mater. *128*, 111–116.

48. Cape, J.A., and Lehman, G.W. (1971). Magnetic Domain Structures in Thin Uniaxial Plates with Perpendicular Easy Axis. J. Appl. Phys. *42*, 5732–5756.

49. Málek, Z., and Kamberskỳ, V. (1958). On the theory of the domain structure of thin films of magnetically uni-axial materials. Cechoslovackij fiziceskij zurnal *8*, 416–421.

50. Millev, Y. (1996). Bose-einstein integrals and domain morphology in ultrathin ferromagnetic films with perpendicular magnetization. J. Phys. Condens. Matter *8*, 3671–3676.

51. Lemesh, I., Büttner, F., and Beach, G.S.D. (2017). Accurate model of the stripe domain phase of perpendicularly magnetized multilayers. Phys. Rev. B *95*, 174423.

52. Büttner, F., Lemesh, I., Schneider, M., Pfau, B., Günther, C.M., Hessing, P., Geilhufe, J., Caretta, L., Engel, D., Krüger, B., et al. (2017). Field-free deterministic ultrafast creation of magnetic skyrmions by spin–orbit torques. Nat. Nanotechnol. *12*, 1040–1044.

53. Romming, N., Kubetzka, A., Hanneken, C., von Bergmann, K., and Wiesendanger, R. (2015). Field-dependent size and shape of single magnetic skyrmions. Phys. Rev. Lett. *114*, 177203.

54. Boulle, O., Vogel, J., Yang, H., Pizzini, S., de Souza Chaves, D., Locatelli, A., Menteş, T.O., Sala, A., Buda-Prejbeanu, L.D., Klein, O., et al. (2016). Room-temperature chiral magnetic skyrmions in ultrathin magnetic nanostructures. Nat. Nanotechnol. *11*, 449–454.

55. Woo, S., Litzius, K., Krüger, B., Im, M.-Y., Caretta, L., Richter, K., Mann, M., Krone, A., Reeve, R.M., Weigand, M., et al. (2016). Observation of room-temperature magnetic skyrmions and their current-driven dynamics in ultrathin metallic ferromagnets. Nat. Mater. *15*, 501–506.

56. Ostrowski, A. (1969). On the remainder term of the euler-maclaurin formula. J. für die Reine Angewandte Math. (Crelle's J.) *0239–0240*, 268–286.

57. Buchheit, A.A., Keßler, T., Schuhmacher, P.K., and Fauseweh, B. (2023). Exact continuum representation of long-range interacting systems and emerging exotic phases in unconventional superconductors. Phys. Rev. Res. *5*, 043065.

58. Kooy, C. (1960). Experimental and theoretical study of the domain configuration in thin layers of $BaFe_{12}O_{19}$. Philips Res. Rep. *15*.

59. Srivastava, T., Sassi, Y., Ajejas, F., Vecchiola, A., Ngouagnia Yemeli, I., Hurdequint, H., Bouzehouane, K., Reyren, N., Cros, V., Devolder, T., et al. (2023). Resonant dynamics of three-dimensional skyrmionic textures in thin film multilayers. APL Mater. *11*.

60. Liyanage, W.L.N.C., Tang, N., Quigley, L., Borchers, J.A., Grutter, A.J., Maranville, B.B., Sinha, S.K., Reyren, N., Montoya, S.A., Fullerton, E.E., et al. (2023). Three-dimensional structure of hybrid magnetic skyrmions determined by neutron scattering. Phys. Rev. B *107*, 184412.

61. Montoya, S.A., Couture, S., Chess, J.J., Lee, J.C.T., Kent, N., Im, M.-Y., Kevan, S.D., Fischer, P., McMorran, B.J., Roy, S., et al. (2017). Resonant properties of dipole skyrmions in amorphous Fe/Gd multilayers. Phys. Rev. B *95*, 224405.

62. Legrand, W., Chauleau, J.-Y., Maccariello, D., Reyren, N., Collin, S., Bouzehouane, K., Jaouen, N., Cros, V., and Fert, A. (2018). Hybrid chiral domain walls and skyrmions in magnetic multilayers. Sci. Adv. *4*, eaat0415.

63. Hubert, A., and Schäfer, R. (1998). Magnetic Domains: The Analysis of Magnetic Microstructures (Springer Science & Business Media).

64. Sisodia, N., Muduli, P.K., Papanicolaou, N., and Komineas, S. (2021). Chiral droplets and current-driven motion in ferromagnets. Phys. Rev. B *103*, 024431.

65. Reichhardt, C., Reichhardt, C.J.O., and Milošević, M. (2022). Statics and dynamics of skyrmions interacting with disorder and nanostructures. Rev. Mod. Phys. *94*, 035005.

66. Yu, G., Upadhyaya, P., Li, X., Li, W., Kim, S.K., Fan, Y., Wong, K.L., Tserkovnyak, Y., Amiri, P.K., and Wang, K.L. (2016). Room-temperature creation and spin–orbit torque manipulation of skyrmions in thin films with engineered asymmetry. Nano Lett. *16*, 1981–1988.

67. Labrie-Boulay, I., Winkler, T.B., Franzen, D., Romanova, A., Fangohr, H., and Kläui, M. (2024). Machine-learning-based detection of spin structures. Phys. Rev., A. *21*, 014014.

68. Collins, T.J. (2007). Imagej for microscopy. Biotechniques *43*, S25–S30.

69. Horcas, I., Fernández, R., Gomez-Rodriguez, J., Colchero, J., Gómez-Herrero, J., and Baro, A. (2007). WSXM: A software for scanning probe microscopy and a tool for nanotechnology. Rev. Sci. Instrum. *78*, 013705.

70. Lopez-Polin, G., Aramberri, H., Marques-Marchan, J., Weintrub, B.I., Bolotin, K.I., Cerdá, J.I., and Asenjo, A. (2022). High-power-density energy-harvesting devices based on the anomalous nernst effect of co/pt magnetic multilayers. ACS Appl. Energy Mater. *5*, 11835–11843.

71. Vansteenkiste, A., Leliaert, J., Dvornik, M., Helsen, M., Garcia-Sanchez, F., and Van Waeyenberge, B. (2014). The design and verification of MuMax3. AIP Adv. *4*, 107133.